Scientific Research Publishing

Open Journal of Applied Sciences, 2025, 15(4), 1058-1072
https://www.scirp.org/journal/ojapps
ISSN Online: 2165-3925
ISSN Print: 2165-3917

Scattering of SH-Waves by a Circular Inclusion in Exponentially Inhomogeneous Media with Nanoscale-Dependent Density

Yongqiang Sun, Longzhan Liu, Jian Zhang*

Department of Basic Education Research, Xinjiang University of Science and Technology, Kuerle, China
Email: *15009313419@163.com

How to cite this paper: Sun, Y.Q., Liu, L.Z. and Zhang, J. (2025) Scattering of SH-Waves by a Circular Inclusion in Exponentially Inhomogeneous Media with Nanoscale-Dependent Density. *Open Journal of Applied Sciences*, **15**, 1058-1072.
https://doi.org/10.4236/ojapps.2025.154074

Received: March 17, 2025
Accepted: April 20, 2025
Published: April 23, 2025

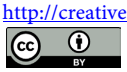

Abstract

Based on complex variable theory, this study investigates the scattering of SH-waves by a circular inclusion in exponentially inhomogeneous media with nanoscale-dependent density and modulus. First, to solve the scattering problem governed by the variable-coefficient Helmholtz equation for a circular inclusion, a conformal mapping method is introduced, transforming the original problem into a standard Helmholtz equation with a circular inclusion. Assuming the medium density varies exponentially along the horizontal direction while the elastic modulus remains constant, explicit analytical expressions are derived for the incident wavefield, scattered wavefield, refracted wavefield within the inclusion, and stress distributions under macroscopic conditions. Second, a generalized boundary condition incorporating nanoscale effects is established using surface elasticity theory. By constructing infinite series equations and leveraging the orthogonality of trigonometric basis functions, numerical solutions for the stress field are rigorously obtained through a truncated series approach. Analysis of the dynamic stress field distribution around the inclusion reveals: 1) Surface elasticity effects significantly alter the stress distribution pattern at the inclusion boundary; 2) The incident wavenumber and inhomogeneity parameter jointly govern the multiscale diffraction characteristics of stress waves.

Keywords

SH Wave, Inhomogeneous Medium, Circular Inclusion, Surface Effect, Dynamic Stress Concentration Factor

1. Introduction

The interaction mechanisms between elastic waves and internal defects (e.g.,

pores, inclusions, and cracks) in materials constitute a fundamental problem in solid mechanics and wave theory. Scattering effects not only induce energy dissipation but also reveal microscopic structural features of materials through frequency-domain information of scattered waves, providing theoretical foundations for seismic engineering, rock mass evaluation, and performance optimization of nanocomposites. Traditional continuum mechanics face significant challenges at the nanoscale: when material characteristic dimensions shrink to the nanoscale, the accumulation of surface energy caused by a dramatic increase in the proportion of surface atoms profoundly alters wave propagation behavior. Consequently, constructing elastic wave scattering models for nanoscale inhomogeneous media and establishing quantitative relationships between circular inclusion-type defects and scattering fields have emerged as frontier topics in multiscale wave theory.

For homogeneous media containing geometric features (e.g., circular holes, spherical/cylindrical inclusions), researchers have uncovered nonlinear correlations between incident wave frequencies and dynamic stress fields (see studies [1]-[3]). Semi-infinite space scattering problems have been resolved using asymptotic matching techniques and Hankel-Bessel series expansions [4] [5]. Research on inhomogeneous media has focused on wave coupling effects in layered interfaces and continuously graded systems. In layered media, shear modulus differences between layers significantly amplify dynamic stress concentration factors [6]-[8]. For elastic wave propagation in continuously inhomogeneous media, Reference [9] pioneered a fundamental solution framework for SH-wave scattering in inhomogeneous anisotropic media, establishing a mathematical foundation for subsequent studies on heterogeneous scattering. Reference [10] developed a generalized Green's function theory for shear wave propagation in anisotropic graded materials, deriving dispersion equations for inhomogeneous layers under point-source excitation via Fourier transform methods. In solving complex inhomogeneous engineering problems, complex variable theory and numerical mapping techniques exhibit unique advantages: Reference [11] formulated dynamic criteria for SH-wave-induced crack propagation by coupling porous media with pre-stress fields; Reference [12] integrated conformal mapping and multipolar coordinate shifting techniques to quantify topological variations in dynamic stress concentration factors caused by interference effects of dual elliptical holes in exponentially graded matrices; References [13]-[15] proposed auxiliary function algorithms that unified variable-coefficient scattering problem frameworks through standard Helmholtz equation transformations, enabling generalized analysis of arbitrary cavity structures in density-graded media. Reference [16] systematically parameterized the coupled effects of wavenumber ratios, modulus ratios, and reference wavenumbers to elucidate multiscale dynamic stress concentration mechanisms around circular inclusions. References [17]-[20] further established full-dimensional parametric characterization spaces (inhomogeneity coefficients, dimensionless wavenumbers, shallow burial depths), refining universal predictive models for dynamic

stress focusing on heterogeneous systems.

At the nanoscale, the increased proportion of surface atoms leads to substantial surface energy accumulation, rendering classical continuum theories inadequate for characterizing surface effects on wave propagation. Reference [21] proposed a zero-thickness surface film model, establishing a theoretical framework for non-classical boundary conditions incorporating surface residual stresses. Experimental validations of this framework were provided in References [22] [23]. References [24] [25] developed analytical models for elastic wave scattering involving nanoscale cylindrical voids/inclusions using wave function expansion methods, systematically revealing strong coupling mechanisms between surface stress tensors and scattering fields of P-, SV-, and SH-waves. These studies demonstrated that dynamic stress concentration factors depend not only on incident wave parameters and bulk material properties but also exhibit significant correlations with nanoscale-specific surface effects. References [26]-[28] investigated elastic wave diffraction around cylindrical nanoscale inclusions via multipolar coordinate shifting techniques, clarifying that nonlinear interactions between interfacial stress gradients and wave phase superposition govern transitions in dynamic stress concentration factors as inclusion spacings shift from near-field strong interference to far-field weak coupling regimes. These findings provide theoretical models for quantifying structure-property relationships in nanoparticle clusters. References [29] [30] addressed asymmetric boundary modeling challenges for nanoscale particle scattering fields in half-space constrained systems using equivalent large-arc mapping principles, proposing a surface-stress-modified dynamic stress concentration factor prediction framework. Results indicated that nanoparticle sizes and interference effects from free-surface reflected waves jointly dominate multimodal scattering field distributions. References [31] [32] employed wave function expansion and complex variable theories to analyze interfacial effects of SH-wave scattering by cylindrical and arbitrarily shaped nanoscale inclusions/cavities. To date, studies on SH-wave scattering by circular inclusions in continuously inhomogeneous media at the nanoscale remain scarce, highlighting the theoretical significance of systematic investigations into this problem.

Considering the complexity of arbitrarily shaped pores and inclusions, this study only establishes a theoretical model for SH-wave scattering by a circular nanoscale inclusion embedded in an infinite inhomogeneous elastic medium, grounded in surface elasticity theory. By leveraging complex variable theory and conformal mapping techniques, analytical expressions for displacement and stress fields are derived. Emphasis is placed on numerical calculations of the dynamic stress concentration factor (DSCF) around the inclusion, with systematic analyses of the influences of surface effects, wavenumbers, and inhomogeneity parameters on the dynamic stress concentration characteristics of the matrix material.

2. Governing Equations

Considering a homogeneous isotropic linearly elastic body with volume V and

surface area S. Let the mass density be ρ, the body force per unit mass (excluding inertial forces) acting on the interior be f_i, the traction per unit area on the outer surface S be p_i, and the displacement of material points be u_i. By applying Gauss's theorem to convert surface integrals into volume integrals, the governing equation for the dynamic problem can be derived as

$$\sigma_{ij,j} + \rho f_i = \rho \frac{\partial^2 u_i}{\partial t^2} \tag{1}$$

$$\sigma_{ij} = \lambda \varepsilon_{kk} \delta_{ij} + 2\mu \varepsilon_{ij} \tag{2}$$

$$\varepsilon_{ij} = \frac{1}{2}\left(u_{i,j} + u_{j,i}\right) \tag{3}$$

here, Equation (1) is called the equation of motion, while Equations (2) and (3) are referred to as the constitutive equation and geometric equation, respectively. $\lambda = B - 2\mu/3$, λ and μ are known as the Lamé constants. B represents the bulk modulus of the linear elastic material. σ_{ij} denotes the stress tensor of the matrix, and ε_{ij} indicates the strain tensor of the matrix.

Considering anti-plane shear motion, we have $u_1 = u_2 = 0, u_3 = w(x, y, t)$. Due to this pure shear state, the stress-strain relationship of the linear elastic material is simplified accordingly. Neglecting body forces, its dynamic governing equation can then be reduced to

$$\frac{\partial \sigma_{xz}}{\partial x} + \frac{\partial \sigma_{yz}}{\partial y} = \rho \frac{\partial^2 w}{\partial t^2} \tag{4}$$

$$\sigma_{xz} = \mu \frac{\partial w}{\partial x},\ \sigma_{yz} = \mu \frac{\partial w}{\partial y} \tag{5}$$

here, σ_{xz}, σ_{yz} represent the shear stresses in the matrix.

By substituting Equation (5) into Equation (4) and assuming $w = W(x, y)\exp(-\mathrm{i}\omega t)$, the anti-plane wave equation in a homogeneous and isotropic medium can be derived

$$\nabla^2 W(x, y) + k^2 W(x, y) = 0 \tag{6}$$

here, ∇^2 is the Laplacian operator, $k = \omega/c$ denotes the wavenumber, $c = \sqrt{\mu/\rho}$ represents the shear wave velocity of the matrix, and ω corresponds to the angular frequency.

Assuming the density function of the medium varies continuously and exponentially along a specific spatial coordinate axis while the elastic modulus remains constant, the mathematical expression for the density can be formulated as

$$\rho(x) = \rho_0 \beta^2 \exp(2\beta x) \tag{7}$$

where ρ_0 is the reference density of the medium, and β denotes the inhomogeneity coefficient.

Furthermore, the wavenumber of the inhomogeneous medium can be derived as

$$k(x) = k_0 \beta \exp(\beta x) \tag{8}$$

here, $k_0 = \omega\sqrt{\rho_0/\mu}$ is the reference wavenumber of the medium.

According to Equation (6), the variable-coefficient wave equation in this medium can be expressed as

$$\nabla^2 W(x,y) + k_0^2 \beta^2 \exp(2\beta x) W(x,y) = 0 \tag{9}$$

Based on the theory of complex variables and by introducing a pair of conjugate complex variables $z = x + \mathrm{i}y$ and $z = x - \mathrm{i}y$, Equation (9) can be reformulated as

$$\frac{\partial^2 W}{\partial z \partial \bar{z}} + \frac{1}{4} k_0^2 \beta^2 \exp\left[\beta\left(z + \bar{z}\right)\right] W = 0 \tag{10}$$

To solve Equation (10), the following conformal mapping is introduced

$$\chi = \omega(z) = \mathrm{e}^{\beta z}, \quad \bar{\chi} = \overline{\omega(z)} = \mathrm{e}^{\beta \bar{z}} \tag{11}$$

By substituting Equation (11) into Equation (10), the standard Helmholtz equation can be derived as

$$\frac{\partial^2 W}{\partial \chi \partial \bar{\chi}} + \frac{1}{4} k_0^2 W = 0 \tag{12}$$

3. Displacement and Stress Fields

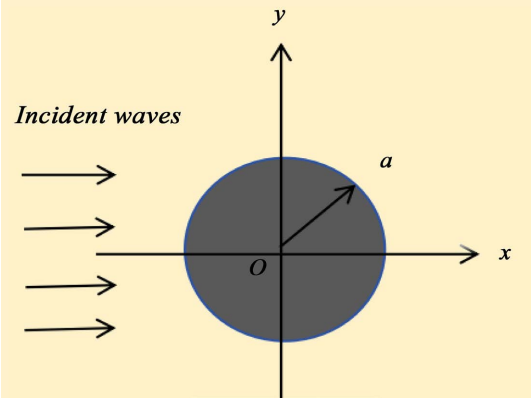

Figure 1. Model of elastic shear wave incident along the positive *x*-axis in an infinite inhomogeneous medium.

As shown in **Figure 1**, assuming the incident wave propagates along the positive horizontal direction in the matrix, its mathematical expression can be derived as follows

$$W^{(\mathrm{inc})} = W_0 \exp\left[\mathrm{i}k_1\left(\chi + \bar{\chi}\right)/2\right] \tag{13}$$

where, W_0 is the wave amplitude, and k_1 is the reference wave speed in the matrix.

The scattered wave caused by inclusions satisfies Equation (12), and the specific form can be

$$W^{(\mathrm{sca})} = \sum_{n=-\infty}^{\infty} A_n H_n^{(1)}\left(k_1 |\chi|\right)\left[\frac{\chi}{|\chi|}\right]^n \tag{14}$$

where $H_n^{(1)}(\cdot)$ is the *n*-th order Hankel function of the first kind, and A_n is the unknown coefficient in the algebraic equation.

The expression for the standing wave excited within the circular inclusion can be written in the following form

$$W^{(\mathrm{fra})} = \sum_{n=-\infty}^{\infty} B_n J_n\left(k_2|\chi|\right)\left[\frac{\chi}{|\chi|}\right]^n \tag{15}$$

where $J_n(\cdot)$ is the *n*-th order Bessel function of the first kind, and B_n is the unknown coefficient in the algebraic equation.

According to Equation (5), the stress in plane z can be expressed as

$$\sigma_{rz} = \mu\left(\frac{\partial W}{\partial z}\mathrm{e}^{\mathrm{i}\theta} + \frac{\partial W}{\partial \overline{z}}\mathrm{e}^{-\mathrm{i}\theta}\right) \tag{16}$$

$$\sigma_{\theta z} = \mathrm{i}\mu\left(\frac{\partial W}{\partial z}\mathrm{e}^{\mathrm{i}\theta} - \frac{\partial W}{\partial \overline{z}}\mathrm{e}^{-\mathrm{i}\theta}\right) \tag{17}$$

Substituting Equation (11) into Equations (16) and (17), the shear stress components can be expressed as

$$\sigma_{rz} = \mu\beta\left(\frac{\partial W}{\partial \chi}\chi\mathrm{e}^{\mathrm{i}\theta} + \frac{\partial W}{\partial \overline{\chi}}\overline{\chi}\mathrm{e}^{-\mathrm{i}\theta}\right) \tag{18}$$

$$\sigma_{\theta z} = \mathrm{i}\mu\beta\left(\frac{\partial W}{\partial \chi}\chi\mathrm{e}^{\mathrm{i}\theta} - \frac{\partial W}{\partial \overline{\chi}}\overline{\chi}\mathrm{e}^{-\mathrm{i}\theta}\right) \tag{19}$$

For the incident wave (13), through equations (18) and (19), the shear stress components can be formulated as

$$\sigma_{rz}^{(\mathrm{inc})} = \frac{\mathrm{i}}{2}\mu_1\beta k_1 W_0\left[\chi\mathrm{e}^{\mathrm{i}\theta} + \overline{\chi}\mathrm{e}^{-\mathrm{i}\theta}\right]\exp\left\{\mathrm{i}k_1\left[\chi + \overline{\chi}\right]/2\right\} \tag{20}$$

$$\sigma_{\theta z}^{(\mathrm{inc})} = -\frac{1}{2}\mu_1\beta k_1 W_0\left[\chi\mathrm{e}^{\mathrm{i}\theta} - \overline{\chi}\mathrm{e}^{-\mathrm{i}\theta}\right]\exp\left\{\mathrm{i}k_1\left[\chi + \overline{\chi}\right]/2\right\} \tag{21}$$

Similarly, for the scattered wave (14), the shear stress components can be formulated as

$$\sigma_{rz}^{(\mathrm{sca})} = \frac{1}{2}\mu_1\beta k_1\sum_{n=-\infty}^{\infty} A_n\left\{H_{n-1}^{(1)}\left(k_1|\chi|\right)\left[\frac{\chi}{|\chi|}\right]^{n-1}\cdot\chi\mathrm{e}^{\mathrm{i}\theta} - H_{n+1}^{(1)}\left(k_1|\chi|\right)\left[\frac{\chi}{|\chi|}\right]^{n+1}\cdot\overline{\chi}\mathrm{e}^{-\mathrm{i}\theta}\right\} \tag{22}$$

$$\sigma_{\theta z}^{(\mathrm{sca})} = \frac{\mathrm{i}}{2}\mu_1\beta k_1\sum_{n=-\infty}^{\infty} A_n\left\{H_{n-1}^{(1)}\left(k_1|\chi|\right)\left[\frac{\chi}{|\chi|}\right]^{n-1}\cdot\chi\mathrm{e}^{\mathrm{i}\theta} + H_{n+1}^{(1)}\left(k_1|\chi|\right)\left[\frac{\chi}{|\chi|}\right]^{n+1}\cdot\overline{\chi}\mathrm{e}^{-\mathrm{i}\theta}\right\} \tag{23}$$

For the standing wave (15) excited within the circular inclusion, the shear stress components can be formulated as

$$\sigma_{rz}^{(\mathrm{fra})} = \frac{1}{2}\mu_2\beta k_2\sum_{n=-\infty}^{\infty} B_n\left\{J_{n-1}\left(k_2|\chi|\right)\left[\frac{\chi}{|\chi|}\right]^{n-1}\cdot\chi\mathrm{e}^{\mathrm{i}\theta} - J_{n+1}^{(1)}\left(k_2|\chi|\right)\left[\frac{\chi}{|\chi|}\right]^{n+1}\cdot\overline{\chi}\mathrm{e}^{-\mathrm{i}\theta}\right\} \tag{24}$$

$$\sigma_{\theta z}^{(\mathrm{fra})}=\frac{\mathrm{i}}{2}\mu_2\beta k_2\sum_{n=-\infty}^{\infty}B_n\left\{J_{n-1}\left(k_2|\chi|\right)\left[\frac{\chi}{|\chi|}\right]^{n-1}\cdot\chi\mathrm{e}^{\mathrm{i}\theta}+J_{n+1}^{(1)}\left(k_2|\chi|\right)\left[\frac{\chi}{|\chi|}\right]^{n+1}\cdot\overline{\chi}\mathrm{e}^{-\mathrm{i}\theta}\right\} \tag{25}$$

4. Surface Elasticity Theory and Boundary Conditions

Based on the interaction between the matrix and the inclusion, under macroscopic conditions, the displacement and stress at boundary $r=a$ must satisfy

$$\begin{cases}W^{(M)}=W^{(I)}\\ \sigma_{rz}^{(M)}=\sigma_{rz}^{(I)}\end{cases} \tag{26}$$

where $W^{(M)}=W^{(\mathrm{inc})}+W^{(\mathrm{sca})}$, $W^{(I)}=W^{(\mathrm{fra})}$, $\sigma_{rz}^{(M)}=\sigma_{rz}^{(\mathrm{inc})}+\sigma_{rz}^{(\mathrm{sca})}$, $\sigma_{rz}^{(I)}=\sigma_{rz}^{(\mathrm{fra})}$.

In surface elasticity theory, a free surface is modeled as an elastic membrane of negligible thickness that is perfectly bonded to the bulk material matrix without slip. In this case, the interior of the solid bulk material follows the same equilibrium equations and constitutive equations as classical elasticity theory. However, the presence of surface stress introduces non-classical boundary conditions [21]. Generally, the surface stress tensor $\sigma_{\alpha\beta}^{s}$ and the surface energy density $E\left(\varepsilon_{\alpha\beta}\right)$ are related as follows

$$\sigma_{\alpha\beta}^{s}=\tau^{0}\delta_{\alpha\beta}+\frac{\partial E}{\partial\varepsilon_{\alpha\beta}} \tag{27}$$

In the equation, $\delta_{\alpha\beta}$ represents the Kronecker delta, $\varepsilon_{\alpha\beta}$ denotes the second-order surface strain tensor, and τ^{0} is the residual surface tension in the strain-free state. Throughout this paper, the Einstein summation convention is adopted, with summation performed over repeated Latin and Greek letter indices.

According to the generalized Young-Laplace equation [31] [32], the surface/interface equilibrium equations are

$$\left(\sigma^{(M)}-\sigma^{(I)}\right)\boldsymbol{n}=-\nabla_{s}\cdot\sigma^{(s)} \tag{28}$$

where $\sigma^{(M)}$, $\sigma^{(I)}$, and $\sigma^{(s)}$ denote the stress tensors of the matrix, inclusion, and surface, respectively; $\boldsymbol{n}$ is the unit normal vector; and $\nabla_{s}\cdot\sigma^{(s)}$ represents the divergence of the surface stress tensor $\sigma^{(s)}$.

The constitutive relationship between the surface stress tensor and the strain tensor is derived using elasticity theory and tensor analysis

$$\sigma_{\alpha\beta}^{(s)}=\tau^{0}\delta_{\alpha\beta}+2\left(\mu^{(s)}-\tau^{0}\right)\delta_{\alpha\gamma}\varepsilon_{\gamma\beta}+\left(\lambda^{(s)}+\tau^{0}\right)\varepsilon_{\gamma\gamma}\delta_{\alpha\beta} \tag{29}$$

where $\mu^{(s)}$ and $\lambda^{(s)}$ are surface parameters.

By combining Equations (1)-(3) and (27)-(29), the boundary conditions on a circular inclusion of radius a at the nanoscale can be obtained as

$$\begin{cases}W^{(M)}=W^{(I)}\\ \sigma_{rz}^{(M)}-\sigma_{rz}^{(I)}=-s\dfrac{\partial\sigma_{\theta z}^{(M)}}{\partial\theta}\end{cases} \tag{30}$$

where $\sigma_{\theta z}^{(M)} = \sigma_{\theta z}^{(\mathrm{inc})} + \sigma_{\theta z}^{(\mathrm{sca})}$, $s = \dfrac{\mu^{(s)}}{a\mu}$, and s is a parameter reflecting the nanoscale effects of the surface/interface. It can be observed that for a specific elastomer material system, the dimensionless parameter s exhibits an inverse proportionality to the pore radius a. When the material operates at the macroscopic scale, the value of parameter s approaches negligible magnitudes. In this regime, the influence of surface energy effects becomes insignificant compared to volumetric strain energy, which aligns with the fundamental assumptions of classical continuum mechanics. However, when the characteristic material dimensions enter the nanoscale regime, parameter s increases by orders of magnitude. At this scale, the surface stress tensor becomes comparable in magnitude to the bulk stress tensor. To accurately describe the mechanical response of the material, it is imperative to incorporate surface elasticity theory and modify the traditional constitutive relations.

By substituting Equations (13)-(15) and Equations (20)-(25) into the boundary condition Equation (30) and simplifying, we obtain

$$\begin{cases} \sum_{n=-\infty}^{\infty} \left[A_n \Theta_n^{(11)} + B_n \Theta_n^{(12)} \right] = \Theta^{(1)} \\ \sum_{n=-\infty}^{\infty} \left[A_n \Theta_n^{(21)} + B_n \Theta_n^{(22)} \right] = \Theta^{(2)} \end{cases} \tag{31}$$

where $\Theta_n^{(11)}, \Theta_n^{(12)}, \Theta^{(1)}, \Theta_n^{(21)}, \Theta_n^{(22)}, \Theta^{(2)}$ is provided in the **Appendix**.

By multiplying both sides of Equation (31) by $\mathrm{e}^{-\mathrm{i}m\theta}$ and integrating over the interval $(-\pi, \pi)$, we obtain

$$\begin{cases} \begin{bmatrix} \Theta_{mn}^{(11)} & \Theta_{mn}^{(12)} \\ \Theta_{mn}^{(21)} & \Theta_{mn}^{(22)} \end{bmatrix} \begin{bmatrix} A_n \\ B_n \end{bmatrix} = \begin{bmatrix} \Theta_m^{(1)} \\ \Theta_m^{(2)} \end{bmatrix} \end{cases} \quad m = 0, \pm 1, \pm 2, \cdots \tag{32}$$

where

$$\begin{cases} \Theta_{mn}^{(11)} = \dfrac{1}{2\pi} \int_{-\pi}^{\pi} \Theta_n^{(11)} \mathrm{e}^{-\mathrm{i}m\theta} \mathrm{d}\theta, \ \Theta_{mn}^{(12)} = \dfrac{1}{2\pi} \int_{-\pi}^{\pi} \Theta_n^{(12)} \mathrm{e}^{-\mathrm{i}m\theta} \mathrm{d}\theta, \\ \Theta_m^{(1)} = \dfrac{1}{2\pi} \int_{-\pi}^{\pi} \Theta^{(1)} \mathrm{e}^{-\mathrm{i}m\theta} \mathrm{d}\theta, \ \Theta_{mn}^{(21)} = \dfrac{1}{2\pi} \int_{-\pi}^{\pi} \Theta_n^{(21)} \mathrm{e}^{-\mathrm{i}m\theta} \mathrm{d}\theta, \\ \Theta_{mn}^{(22)} = \dfrac{1}{2\pi} \int_{-\pi}^{\pi} \Theta_n^{(22)} \mathrm{e}^{-\mathrm{i}m\theta} \mathrm{d}\theta, \ \Theta_m^{(2)} = \dfrac{1}{2\pi} \int_{-\pi}^{\pi} \Theta^{(2)} \mathrm{e}^{-\mathrm{i}m\theta} \mathrm{d}\theta \end{cases} \tag{33}$$

5. Numerical Results and Discussion

This study focuses on analyzing the dynamic stress concentration phenomenon around circular inclusions. The Dynamic Stress Concentration Factor (DSCF) is defined as the ratio of stress component $\sigma_{\theta z}^{(M)}$ to the reference stress σ_0. This factor can be determined using the following expression

$$\mathrm{DSCF} = \left| \sigma_{\theta z}^{(M)} / \sigma_0 \right| \tag{34}$$

where $\sigma_0 = \mu_1 k_1 W_0$ is the stress intensity in the propagation direction of the SH wave.

Substituting Equations (21) and (23) into Equation (34) yields the final DSCF result

$$\mathrm{DSCF}=-\frac{1}{2}\left(\chi \mathrm{e}^{\mathrm{i}\theta}-\overline{\chi}\mathrm{e}^{-\mathrm{i}\theta}\right)\exp\left\{\mathrm{i}k_1\left[\chi+\overline{\chi}\right]/2\right\}+\frac{\mathrm{i}}{2}\sum_{n=-\infty}^{\infty}A_n\left\{H_{n-1}^{(1)}\left(k_1|\chi|\right)\left[\frac{\chi}{|\chi|}\right]^{n-1}\cdot\chi\mathrm{e}^{\mathrm{i}\theta}+H_{n+1}^{(1)}\left(k_1|\chi|\right)\left[\frac{\chi}{|\chi|}\right]^{n+1}\cdot\overline{\chi}\mathrm{e}^{-\mathrm{i}\theta}\right\} \tag{35}$$

Based on the theoretical derivation above, the following section focuses on the distribution of dynamic stress concentration around a circular inclusion in a heterogeneous infinite medium at the nanoscale. The following dimensionless definitions are adopted: Matrix reference wavenumber k_1a, Heterogeneity parameter βa, Surface parameter s, Wavenumber ratio between the matrix and inclusion $k^*=k_2/k_1$, Shear modulus ratio $\mu^*=\mu_1/\mu_2$. Three distinct cases are selected as numerical examples for comparative analysis: 1) $k^*=0.5$, $\mu^*=0.25$; 2) $k^*=2.0$, $\mu^*=4.0$; 3) $k^*=4.0$, $\mu^*=16.0$, representing scenarios where the inclusion is relatively stiffer, softer, and even softer than the matrix, respectively.

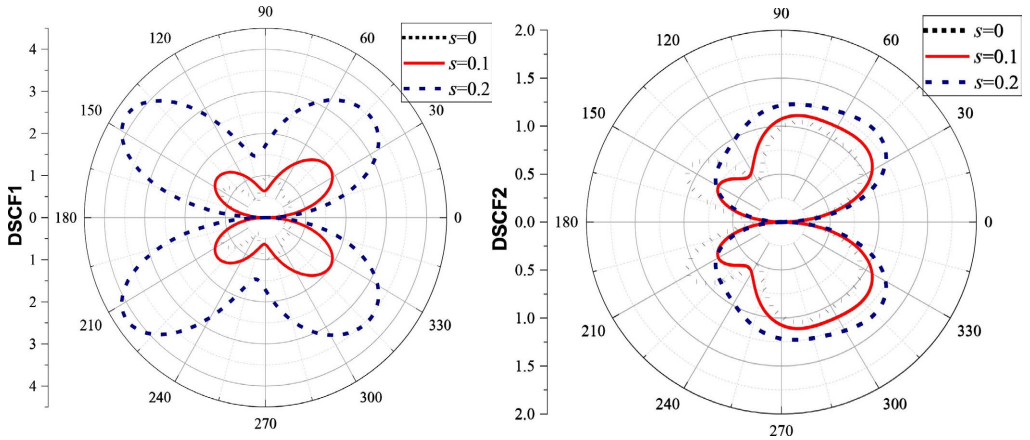

(a) $k^*=0.5, \mu^*=0.25$ (b) $k^*=2.0, \mu^*=4.0$

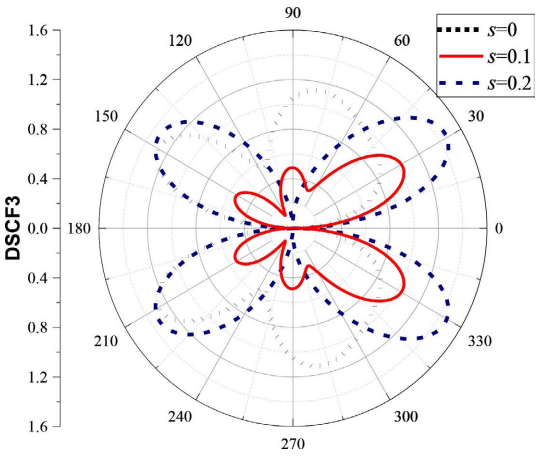

(c) $k^*=4.0, \mu^*=16$

Figure 2. Variation of DSCF around the circular inclusion with the surface parameter s ($\beta a=1.0$).

Figure 2 presents the distribution of the dynamic stress concentration factor (DSCF) around the circular inclusion in an exponentially graded heterogeneous medium under a horizontally incident elastic shear wave, with βa set to 1, for different values of the wavenumber ratio k^* and shear modulus ratio μ^*, as functions of the surface parameter s. It can be visually observed that the DSCF exhibits a symmetric distribution pattern. As the surface parameter s increases, the DSCF significantly increases. Furthermore, the figure reveals that the relative stiffness between the matrix and the inclusion substantially influences the DSCF distribution.

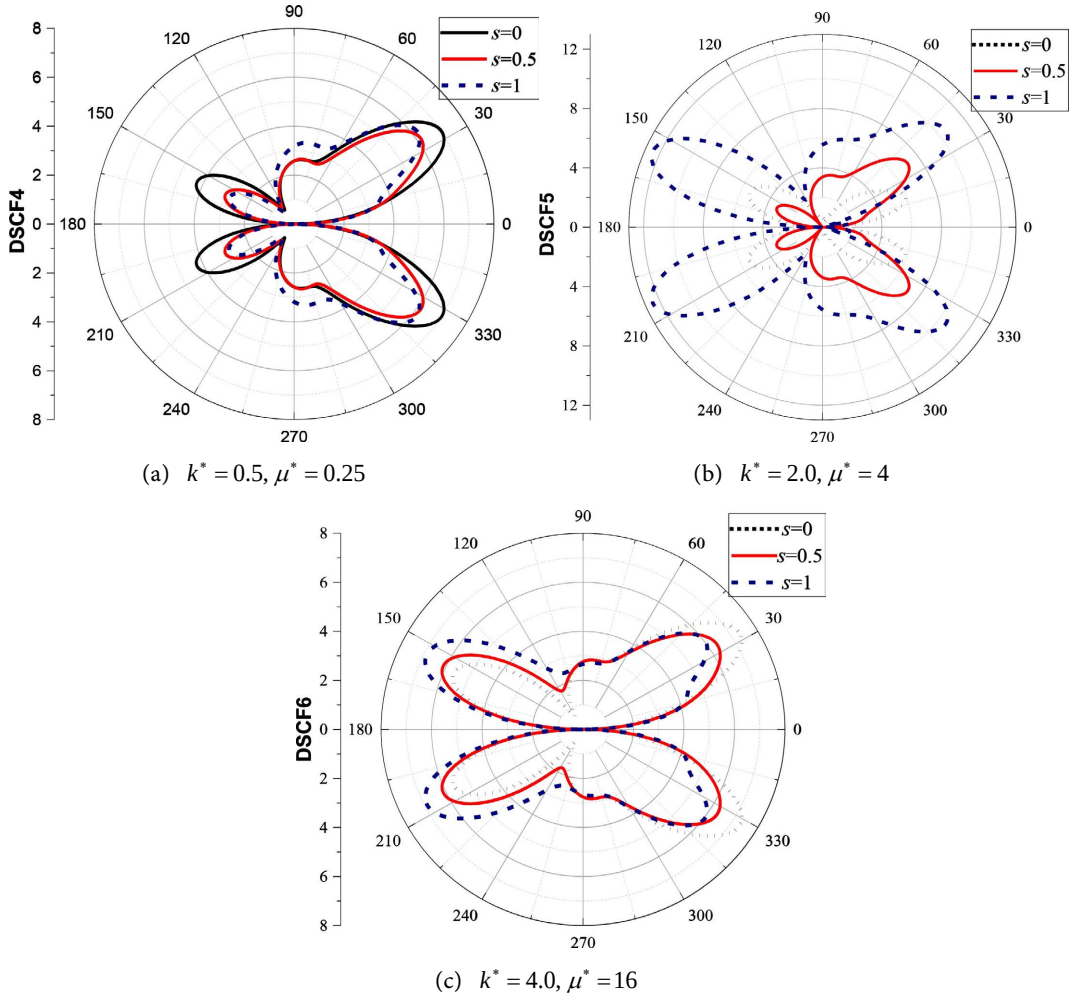

(a) $k^* = 0.5, \mu^* = 0.25$ (b) $k^* = 2.0, \mu^* = 4$

(c) $k^* = 4.0, \mu^* = 16$

Figure 3. Variation of DSCF around the circular inclusion with the surface parameter s ($\beta a = 2.0$).

Figure 3 illustrates the distribution of the dynamic stress concentration factor (DSCF) around the circular inclusion in an exponentially graded heterogeneous medium under a horizontally incident elastic shear wave, with βa set to 2, for varying wavenumber ratios k^* and shear modulus ratios μ^*, plotted against the surface parameter s. Visually, the DSCF exhibits a symmetric distribution. As s increases, the DSCF notably amplifies. Additionally, the relative stiffness

contrast between the matrix and inclusion significantly affects the DSCF profile. Compared to Figure 2, where the heterogeneity parameter is $\beta a = 1.0$, the DSCF values in Figure 3 (with $\beta a = 2.0$) are universally higher, demonstrating the pronounced impact of the heterogeneity parameter on dynamic stress concentration.

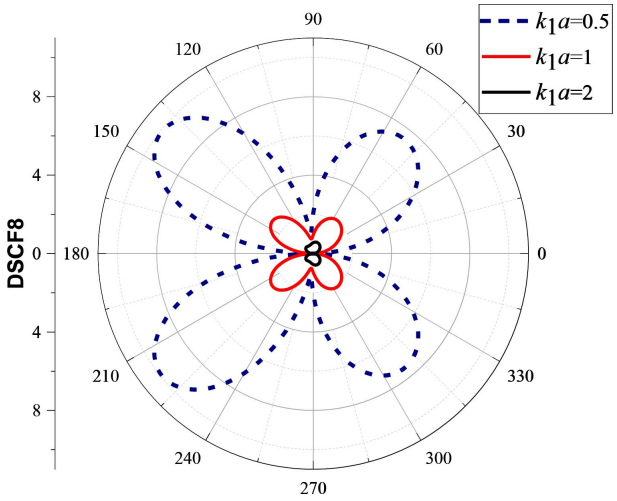

$\beta a = 0.5, k^* = 2.0, \mu^* = 16, s = 0.1$

Figure 4. Distribution of DSCF around the circular inclusion as a function of the matrix reference wavenumber k_1a.

Figure 4 presents the distribution of the dynamic stress concentration factor (DSCF) around the circular inclusion in an exponentially graded heterogeneous medium under the condition $\beta a = 0.5$, $k^* = 2.0$, $\mu^* = 16$, $s = 0.1$, for different values of the matrix reference wavenumber k_1a. It can be visually observed that the DSCF exhibits a symmetric distribution pattern. As the matrix reference wavenumber k_1a increases, the DSCF decreases.

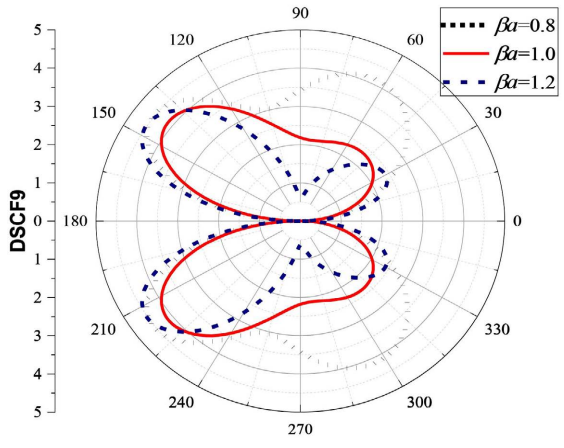

$k^* = 0.5, \mu^* = 0.25, s = 0.5$

Figure 5. Distribution of DSCF around the circular inclusion as a function of the heterogeneity parameter βa.

Figure 5 illustrates the distribution of the dynamic stress concentration factor (DSCF) around the circular inclusion in an exponentially graded heterogeneous medium under the condition $k^* = 0.5$, $\mu^* = 0.25$, $s = 0.5$, for varying values of the heterogeneity parameter βa. It can be visually observed that the DSCF exhibits a symmetric distribution pattern. As the heterogeneity parameter βa increases, the DSCF undergoes discernible variations.

6. Conclusions

This study, grounded in the theory of complex functions, investigates the scattering of incident SH waves by Cylindrical nano-scale inclusion within an infinitely large density inhomogeneous medium. Numerical examples were employed to analyze the influence of Matrix reference wavenumber $k_1 a$, Heterogeneity parameter βa, Surface parameter s, Wavenumber ratio between the matrix and inclusion $k^* = k_2/k_1$, Shear modulus ratio $\mu^* = \mu_1/\mu_2$. The following conclusions were drawn:

1) The dynamic stress concentration factor around the inclusion changes significantly with an increase in surface effects.

2) Changes in inhomogeneous parameters lead to notable variations in the dynamic stress concentration factor.

3) The dynamic stress concentration factor decreases progressively with changes in the Heterogeneity parameter.

These analyses and discussions provide theoretical support for the fabrication of cylindrical nanomaterials.

7. Outlook

In subsequent research, we will investigate the scattering of elastic waves by arbitrarily shaped inclusions and cavities in more general nonhomogeneous media. We will conduct extensive parametric studies to develop a theoretical model that better aligns with practical applications, thereby contributing to advancements in nanomaterial fabrication.

Conflicts of Interest

The authors declare no conflicts of interest regarding the publication of this paper.

References

[1] Baron, M.L. and Matthews, A.T. (1961) Diffraction of a Pressure Wave by a Cylindrical Cavity in an Elastic Medium. *Journal of Applied Mechanics*, **28**, 347-354. https://doi.org/10.1115/1.3641710

[2] Pao, Y.H. and Mow, C.C. (1962) Dynamic Stress Concentration in an Elastic Plate with Rigid Circular Inclusion. *Proceedings of the Fourth US National Congress of Applied Mechanics*, Berkeley, 18-21 June 1962, 335-340.

[3] Pao, Y.H., Mow, C.C. and Achenbach, J.D. (1973) Diffraction of Elastic Waves and Dynamic Stress Concentrations. *Journal of Applied Mechanics*, **40**, 872-872. https://doi.org/10.1115/1.3423178

[4] Datta, S.K. and Shah, A.H. (1982) Scattering of SH Waves by Embedded Cavities. *Wave Motion*, **4**, 265-283. https://doi.org/10.1016/0165-2125(82)90023-3

[5] Davis, C.A., Lee, V.W. and Bardet, J.P. (2001) Transverse Response of Underground Cavities and Pipes to Incident SV Waves. *Earthquake Engineering & Structural Dynamics*, **30**, 383-410. https://doi.org/10.1002/eqe.14

[6] Dravinski, M. and Sheikhhassani, R. (2013) Scattering of a Plane Harmonic SH Wave by a Rough Multilayered Inclusion of Arbitrary Shape. *Wave Motion*, **50**, 836-851. https://doi.org/10.1016/j.wavemoti.2013.02.014

[7] Sheikhhassani, R. and Dravinski, M. (2014) Scattering of a Plane Harmonic SH Wave by Multiple Layered Inclusions. *Wave Motion*, **51**, 517-532. https://doi.org/10.1016/j.wavemoti.2013.12.002

[8] Sheikhhassani, R. and Dravinski, M. (2016) Dynamic Stress Concentration for Multiple Multilayered Inclusions Embedded in an Elastic Half-Space Subjected to SH-waves. *Wave Motion*, **62**, 20-40. https://doi.org/10.1016/j.wavemoti.2015.11.002

[9] Daros, C.H. (2008) A Fundamental Solution for SH-Waves in a Class of Inhomogeneous Anisotropic Media. *International Journal of Engineering Science*, **46**, 809-817. https://doi.org/10.1016/j.ijengsci.2008.02.001

[10] Kumar, P., Chattopadhyay, A. and Singh, A.K. (2017) Shear Wave Propagation Due to a Point Source. *Procedia Engineering*, **173**, 1544-1551. https://doi.org/10.1016/j.proeng.2016.12.241

[11] Singh, A.K., Yadav, R.P., Kumar, S. and Chattopadhyay, A. (2016) Propagation of Crack in a Pre-Stressed Inhomogeneous Poroelastic Medium Influenced by Shear Wave. *Engineering Fracture Mechanics*, **154**, 191-206. https://doi.org/10.1016/j.engfracmech.2015.12.024

[12] Zhou, C., Hu, C., Ma, F. and Liu, D. (2014) Elastic Wave Scattering and Dynamic Stress Concentrations in Exponential Graded Materials with Two Elliptic Holes. *Wave Motion*, **51**, 466-475. https://doi.org/10.1016/j.wavemoti.2013.11.005

[13] Yang, Z., Hei, B. and Wang, Y. (2015) Scattering by Circular Cavity in Radially Inhomogeneous Medium with Wave Velocity Variation. *Applied Mathematics and Mechanics*, **36**, 599-608. https://doi.org/10.1007/s10483-015-1937-7

[14] Hei, B., Yang, Z., Sun, B. and Wang, Y. (2015) Modelling and Analysis of the Dynamic Behavior of Inhomogeneous Continuum Containing a Circular Inclusion. *Applied Mathematical Modelling*, **39**, 7364-7374. https://doi.org/10.1016/j.apm.2015.03.015

[15] Hei, B., Yang, Z., Wang, Y. and Liu, D. (2016) Dynamic Analysis of Elastic Waves by an Arbitrary Cavity in an Inhomogeneous Medium with Density Variation. *Mathematics and Mechanics of Solids*, **21**, 931-940. https://doi.org/10.1177/1081286514545906

[16] Hei, B.P., Yang, Z.L. and Yang, Q.Y. (2015) Dynamic Analysis on a Circular Inclusion in a Radially Inhomogeneous Medium. *Chinese Journal of Theoretical and Applied Mechanics*, **47**, 539-543.

[17] Jiang, G., Yang, Z., Sun, C., Song, Y. and Yang, Y. (2020) Analytical Study of SH Wave Scattering by a Cylindrical Cavity in the Two-Dimensional and Approximately Linear Inhomogeneous Medium. *Waves in Random and Complex Media*, **31**, 1799-1817. https://doi.org/10.1080/17455030.2019.1704308

[18] Jiang, G., Yang, Z., Sun, C., Li, X. and Yang, Y. (2019) Dynamic Stress Concentration of a Cylindrical Cavity in Vertical Exponentially Inhomogeneous Half Space under SH Wave. *Meccanica*, **54**, 2411-2420. https://doi.org/10.1007/s11012-019-01076-2

[19] Yang, Z., Jiang, G., Song, Y., Yang, Y. and Sun, M. (2020) Effect on Dynamic Stress Distribution by the Shape of Cavity in Continuous Inhomogeneous Medium under

SH Waves Incidence. *Mechanics of Advanced Materials and Structures*, **28**, 2071-2082. https://doi.org/10.1080/15376494.2020.1717020

[20] Yang, Z., Jiang, G., Tang, H., Sun, B. and Yang, Y. (2017) Dynamic Analysis of a Cylindrical Cavity in Inhomogeneous Elastic Half-Space Subjected to SH Waves. *Mathematics and Mechanics of Solids*, **24**, 299-311. https://doi.org/10.1177/1081286517739520

[21] Gurtin, M.E. and Ian Murdoch, A. (1975) A Continuum Theory of Elastic Material Surfaces. *Archive for Rational Mechanics and Analysis*, **57**, 291-323. https://doi.org/10.1007/bf00261375

[22] Miller, R.E. and Shenoy, V.B. (2000) Size-Dependent Elastic Properties of Nanosized Structural Elements. *Nanotechnology*, **11**, 139-147. https://doi.org/10.1088/0957-4484/11/3/301

[23] Shenoy, V.B. (2002) Size-Dependent Rigidities of Nanosized Torsional Elements. *International Journal of Solids and Structures*, **39**, 4039-4052. https://doi.org/10.1016/s0020-7683(02)00261-5

[24] Wong, E.W., Sheehan, P.E. and Lieber, C.M. (1997) Nanobeam Mechanics: Elasticity, Strength, and Toughness of Nanorods and Nanotubes. *Science*, **277**, 1971-1975. https://doi.org/10.1126/science.277.5334.1971

[25] Wang, G.F., Wang, T.J. and Feng, X.Q. (2006) Surface Effects on the Diffraction of Plane Compressional Waves by a Nanosized Circular Hole. *Applied Physics Letters*, **89**, Article ID: 231923. https://doi.org/10.1063/1.2403899

[26] Ru, Y., Wang, G.F. and Wang, T.J. (2009) Diffractions of Elastic Waves and Stress Concentration near a Cylindrical Nano-Inclusion Incorporating Surface Effect. *Journal of Vibration and Acoustics*, **131**, Article ID: 061011. https://doi.org/10.1115/1.4000479

[27] Ru, Y., Wang, G.F., Su, L.C. and Wang, T.J. (2013) Scattering of Vertical Shear Waves by a Cluster of Nanosized Cylindrical Holes with Surface Effect. *Acta Mechanica*, **224**, 935-944. https://doi.org/10.1007/s00707-012-0797-7

[28] Yan, R. (2015) Surface Effect on Diffractions of Elastic Waves and Stress Concentration near a Cluster of Cylindrical Nanoholes Arranged as Quadrate Shape. *Advances in Materials Science and Engineering*, **2015**, Article ID: 134975. https://doi.org/10.1155/2015/134975

[29] Fang, X., Zhang, L. and Liu, J. (2011) Dynamic Stress around a Cylindrical Nano-Inhomogeneity with an Interface in a Half-Plane under Anti-Plane Shear Waves. *Applied Physics A*, **106**, 625-633. https://doi.org/10.1007/s00339-011-6633-4

[30] Yang, Q., Liu, J.X. and Fang, X.Q. (2012) Dynamic Stress in a Semi-Infinite Solid with a Cylindrical Nano-Inhomogeneity Considering Nanoscale Microstructure. *Acta Mechanica*, **223**, 879-888. https://doi.org/10.1007/s00707-012-0613-4

[31] Wu, H. (2019) Application of the Complex Variable Function Method to SH-Wave Scattering around a Circular Nanoinclusion. *Advances in Mathematical Physics*, **2019**, Article ID: 7203408. https://doi.org/10.1155/2019/7203408

[32] Wu, H. and Ou, Z. (2019) Surface Effects on the Scattering of SH-Wave around an Arbitrary Shaped Nano-Cavity. *Advances in Mathematical Physics*, **2019**, Article ID: 3084581. https://doi.org/10.1155/2019/3084581

Appendix

$$\Theta_n^{(11)} = H_n^{(1)}\left(k_1|\chi|\right)\left(\frac{\chi}{|\chi|}\right)^n$$

$$\Theta_n^{(12)} = J_n\left(k_1|\chi|\right)\left(\frac{\chi}{|\chi|}\right)^n$$

$$\Theta^{(1)} = -\exp\left[\mathrm{i}k_1\left(\chi+\overline{\chi}\right)/2\right]$$

$$\Theta_n^{(21)} = N_2 - N_3 + s\cdot\mathrm{i}\cdot P_1$$

$$\Theta_n^{(22)} = \frac{\mu_2}{\mu_1}\cdot\frac{k_2}{k_1}\left(N_5 - N_4\right)$$

$$\Theta^{(2)} = s\cdot P_2 - i\cdot N_1$$

$P_1 = \left(M_5+M_6\right)\chi\mathrm{e}^{\mathrm{i}\theta} + M_7 + \left(M_8+M_9\right)\overline{\chi}\mathrm{e}^{-\mathrm{i}\theta} - M_{10}$, $P_2 = \left(M_1 - \overline{M_1}\right)M_2 + M_3M_2M_4$

$M_1 = \chi\beta\mathrm{zie}^{\mathrm{i}\theta} + \chi\mathrm{ie}^{\mathrm{i}\theta}$, $M_2 = \exp\left[\mathrm{i}k_1\left(\chi+\overline{\chi}\right)/2\right]$, $M_3 = \chi\mathrm{e}^{\mathrm{i}\theta} - \overline{\chi}\mathrm{e}^{-\mathrm{i}\theta}$, $M_4 = \frac{\mathrm{i}k_1}{2}\left(\chi\beta\mathrm{zi} - \overline{\chi}\beta\overline{\mathrm{zi}}\right)$,

$M_5 = \frac{k_1}{2}H_{n-2}^{(1)}\left(k_1|\chi|\right)\left(\frac{\chi}{|\chi|}\right)^{n-2}\cdot\chi\beta\mathrm{zi}$, $M_6 = \frac{k_1}{2}H_n^{(1)}\left(k_1|\chi|\right)\left(\frac{\chi}{|\chi|}\right)^{n}\cdot\overline{\chi}\beta\overline{\mathrm{zi}}$, $M_7 = H_{n-1}^{(1)}\left(k_1|\chi|\right)\left(\frac{\chi}{|\chi|}\right)^{n-1}\cdot\left(\chi\beta\mathrm{zie}^{\mathrm{i}\theta} + \chi\mathrm{ie}^{\mathrm{i}\theta}\right)$,

$M_8 = \frac{k_1}{2}H_n^{(1)}\left(k_1|\chi|\right)\left(\frac{\chi}{|\chi|}\right)^{n}\cdot\chi\beta\mathrm{zi}$, $M_9 = \frac{k_1}{2}H_{n+2}^{(1)}\left(k_1|\chi|\right)\left(\frac{\chi}{|\chi|}\right)^{n+2}\cdot\overline{\chi}\beta\overline{\mathrm{zi}}$,

$M_{10} = H_{n+1}^{(1)}\left(k_1|\chi|\right)\left(\frac{\chi}{|\chi|}\right)^{n+1}\cdot\left(\overline{\chi}\beta\overline{\mathrm{zi}}\mathrm{e}^{-\mathrm{i}\theta} + \overline{\chi}\mathrm{ie}^{-\mathrm{i}\theta}\right)$, $N_1 = \left(\chi\mathrm{e}^{\mathrm{i}\theta} + \overline{\chi}\mathrm{e}^{-\mathrm{i}\theta}\right)\exp\left[\mathrm{i}k_1\left(\chi+\overline{\chi}\right)/2\right]$

$N_2 = H_{n-1}^{(1)}\left(k_1|\chi|\right)\left(\frac{\chi}{|\chi|}\right)^{n-1}\cdot\chi\mathrm{e}^{\mathrm{i}\theta}$, $N_3 = H_{n+1}^{(1)}\left(k_1|\chi|\right)\left(\frac{\chi}{|\chi|}\right)^{n+1}\cdot\overline{\chi}\mathrm{e}^{-\mathrm{i}\theta}$, $N_4 = J_{n-1}\left(k_2|\chi|\right)\left(\frac{\chi}{|\chi|}\right)^{n-1}\cdot\chi\mathrm{e}^{\mathrm{i}\theta}$,

$N_5 = J_{n+1}\left(k_1|\chi|\right)\left(\frac{\chi}{|\chi|}\right)^{n+1}\cdot\overline{\chi}\mathrm{e}^{-\mathrm{i}\theta}$